Preprints of the 19th World Congress
The International Federation of Automatic Control
Cape Town, South Africa. August 24-29, 2014

A New Nonlinear Suboptimal Control Design Approach for Milling Circuits

Myrin A. Naidoo * **Radhakant Padhi** [1] * **Ian K. Craig** *

* *Department of Electrical, Electronic and Computer Engineering, University of Pretoria, South Africa.*
(Corresponding author, E-mail: ian.craig@up.ac.za.)

Abstract: A combined nonlinear model predictive control and nonlinear dynamic inversion design approach is proposed as a new effective control design philosophy for complex milling circuits. Nonlinear interaction between various states in the mill and the sump as well as significant time delays make the milling circuit difficult to control. The proposed innovative approach, which uses a suboptimal nonlinear model predictive control for the overall circuit with a fast acting dynamic inversion control for controlling the sump level, addresses the ambitious objectives of high product quality, high throughput, manageable loads in the mill as well as minimum power consumption.

Keywords: Model predictive control, Dynamic inversion, Milling circuit, Run-of-mine mill.

1. INTRODUCTION

A run-of-mine (ROM) ore milling circuit is primarily used to grind incoming precious metal bearing ore to a particle size smaller than about 75 μm (Coetzee et al., 2010). After grinding, the ore is liberated, separated and concentrated in downstream processes. The focus of this paper is to propose a new nonlinear and suboptimal control design approach to produce a high quality milling circuit product, whilst at the same time achieve an adequate throughput with minimum power consumption. Note that the ROM ore milling circuit is a complex process that is difficult to control because of significant nonlinearities, large time delays, large unmeasured disturbances, process variables that are difficult to measure, and modelling uncertainties (Coetzee et al. (2010)).

Traditionally ROM ore milling circuits are controlled by classical single-loop PID controllers (Wei and Craig (2009)), despite the multivariable nature of such circuits. Numerous attempts are noted in the literature, e.g. mu controller designs are described in Craig and MacLeod (1996) and linear model predictive control in Chen et al. (2007).

Recently, an innovative way of controlling the ROM ore milling circuits was proposed using a robust nonlinear model predictive controller (MPC) (Coetzee et al. (2010)). A host of peripheral issues, which are also important for the successful automation of a milling circuit, are described in Olivier et al. (2012) and Olivier and Craig (2013). The main aim of the design methods mentioned above was to maintain a high product quality, i.e. maintain the product particle size at a sufficiently small value. However, throughput and quality are usually inversely proportional (Bauer and Craig (2008)), such that a high quality product leads to a low throughput.

Getting inspired by the work reported in (Coetzee et al. (2010)) and appropriately modifying it, an innovative combined nonlinear model predictive control and nonlinear dynamic inversion design philosophy is presented in this paper. The proposed approach uses a nonlinear MPC control for the overall circuit along with a fast acting dynamic inversion control for controlling the sump level. It addresses the ambitious objectives of high product quality, high throughput, manageable loads in the mill as well as minimum power consumption.

The cost of energy has increased significantly in recent years. This increase in price greatly affects the mineral processing industry due to the large energy demands. A run-of-mine (ROM) ore milling circuit provides a suitable case study where the power consumed by a mill is in the order of 2 MW. Grinding mill circuits have been identified as the most energy and cost intensive unit processes in the minerals processing industry (Wei and Craig (2009)) and hence energy savings can have a substantial impact. In a recent study (Matthews and Craig (2013)), an ROM ore milling circuit was power optimized using a time-of-use (TOU) tariff structure following the concept of demand side management. This study showed that power can be saved by implementing a real time optimizer (RTO) on a supervisory outer-loop level. For regulatory control, a linear model predictive controller (MPC) was used. This paper, on the other hand, tries to save energy in the inner loop by additionally penalizing an energy factor as part of the cost function of the MPC design, and hence is fundamentally different from the RTO philosophy described in Matthews and Craig (2013).

[1] The author works as an Associate Professor in the Dept. of Aerospace Engineering, Indian Institute of Science, Bangalore, India. This work was done while he was a visiting professor at the University of Pretoria, South Africa.

2. RUN-OF-MINE ORE MILLING CIRCUIT MODEL

2.1 Description of the run-of-mine ore milling circuit

The goal of minerals processing is to convert raw ore to a final product. The final product has a higher concentration of the most valuable minerals. The ROM circuit is the focus of this study and is shown in Fig. 1. This circuit forms part of the minerals liberation process.

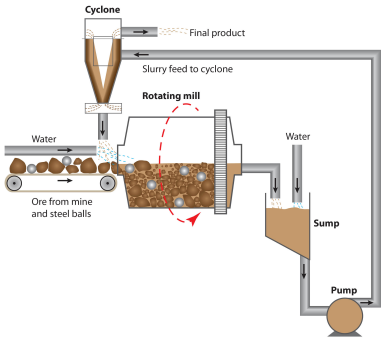

Fig. 1. Run-of-mine circuit. From Le Roux et al. (2013)

Ore containing some valuable mineral (such as those containing copper, iron, platinum or gold) is fed into the mill where it is ground fine using rocks and steel balls as the grinding medium. The mill discharges into a sump where the slurry is diluted with water to achieve the correct density before it is pumped to a hydrocyclone. The cyclone separates the coarse and fine particles, with the fine particles leaving the circuit as product whilst the coarse particles are recycled back into the mill for further grinding.

2.2 Controlled and manipulated variables

All operating points and parameters implemented in this paper can be found in Coetzee et al. (2010). Table 1 shows the constraints and operating values for the manipulated variables (MVs) and controlled variables (CVs). Note that the MVs are the inputs to the system and the CVs are the outputs.

CVs (Outputs) for the ROM are typically the particle size estimate (PSE), percentage of the mill volume filled (LOAD), sump volume (SVOL) and cyclone feed density (CFD) (Matthews and Craig (2013)). In this study, another control variable was introduced, namely throughput (THP).

2.3 State space description

An individual model for each module, shown in Fig. 1, has been created in the past (Coetzee et al. (2010)) and validated using real plant data by Le Roux et al. (2013). The mill has five states, namely water, rocks, solids, fines and steel balls. The sump has an additional three states, namely water, fines and solids. The variables and nomenclature used in this section are shown in Table 1 and Table 2 respectively. The full state space description is shown in (1)-(14) to illustrate the complexity and nonlinearity of the circuit. A time delay of thirty seconds

Table 1. Constraints and operating point

Variable	Min	Max	OP	Description
States				
X_{mw}	0	50	8.28	The volume of water in the mill [m^3]
X_{ms}	0	50	9.51	The volume of ore in the mill [m^3]
X_{mf}	0	50	3.34	The volume of fine ore in the mill [m^3]
X_{mr}	0	50	20.90	The volume of rock in the mill [m^3]
X_{mb}	0	20	6.32	The volume of balls in the mill [m^3]
X_{sw}	0	10	2.53	The volume of water in the sump [m^3]
X_{ss}	0	10	0.64	The volume of ore in the sump [m^3]
X_{sf}	0	10	0.23	The volume of fine ore in the sump [m^3]
MVs				
MIW	0	100	27.17	Flow rate of water to the mill [m^3/h]
MFS	0	200	88.20	Flow rate of solids to the mill [t/h]
MFB	0	4	2	Flow rate of steel balls to the mill [t/h]
CFF	400	500	423.11	Flow rate of slurry to the cyclone [m^3/h]
SFW	0	400	261.62	Flow rate of water to the sump [m^3/h]
α_{speed}	0	100	82	Percentage of critical mill speed [%]
CVs				
PSE	60	90	80	Product particle size [% < 75 μm]
LOAD	30	50	45	Total charge of the mill [%]
SVOL	2	9.5	3	Level of the sump [m^3]
THP	0	200	88	Throughput (coarse and fine solids) [t/h]
CFD	1	2	1344	Cyclone feed density [kg/m^3]

and ten seconds are present between the sump-to-cyclone and cyclone-to-mill respectively.

Mill state equations

$$\dot{X_{mw}} = MIW - \frac{V_V \varphi X_{mw} X_{mw}}{X_{ms} + X_{mw}} + V_{cwu} \tag{1}$$

$$\dot{X_{ms}} = \frac{MFS}{D_S}(1-\alpha_r) - \frac{V_V \varphi X_{mw} X_{ms}}{X_{ms} + X_{mw}} + \frac{P_{mill}\varphi}{D_S \phi_r}\left(\frac{X_{mr}}{X_{mr}+X_{ms}}\right) + V_{csu} \tag{2}$$

$$\dot{X_{mf}} = \frac{MFS}{D_S}\alpha_f - \frac{V_V \varphi X_{mw} X_{mf}}{X_{ms} + X_{mw}} + V_{cfu} + \frac{P_{mill}}{D_S \phi_f \left[1 + \alpha_{\phi_f}\left(\frac{X_{mw}+X_{mr}+X_{ms}+X_{mb}}{v_{mill}} - v_{P_{max}}\right)\right]} \tag{3}$$

$$\dot{X_{mr}} = \frac{MFS}{D_S}\alpha_r - \frac{P_{mill}\varphi}{D_S \phi_r}\left(\frac{X_{mr}}{X_{mr}+X_{ms}}\right) \tag{4}$$

$$\dot{X_{mb}} = \frac{MFB}{D_B} - \frac{P_{mill}\varphi}{\phi_b}\left(\frac{X_{mb}}{D_S\left(X_{mr}+X_{ms}\right) + D_B X_{mb}}\right) \tag{5}$$

Sump state equations

$$\dot{X_{sw}} = \frac{V_V \varphi X_{mw} X_{mw}}{X_{ms} + X_{mw}} - \frac{CFF X_{sw}}{X_{sw} + X_{ss}} + SFW \tag{6}$$

$$\dot{X_{ss}} = \frac{V_V \varphi X_{mw} X_{ms}}{X_{ms} + X_{mw}} - \frac{CFF X_{ss}}{X_{sw} + X_{ss}} \tag{7}$$

$$\dot{X_{sf}} = \frac{V_V \varphi X_{mw} X_{mf}}{X_{ms} + X_{mw}} - \frac{CFF X_{sf}}{X_{sw} + X_{ss}} \tag{8}$$

The circuit contains six outputs shown in (9)-(14).

$$P_{mill} = P_{max} \cdot (1 - \delta_{Pv} Z_x^2 - 2\chi_P \delta_{Pv} \delta_{Ps} Z_x Z_r - \delta_{Ps} Z_r^2)(\alpha_{speed})^{\alpha_P} \tag{9}$$

$$LOAD = X_{mw} + X_{ms} + X_{mr} + X_{mb} \tag{10}$$

$$SVOL = X_{ss} + X_{sw} \tag{11}$$

$$CFD = \frac{X_{sw} + X_{ss} D_S}{X_{sw} + X_{ss}} \tag{12}$$

$$PSE = \frac{V_{cfo}}{V_{cso}} \tag{13}$$

$$THP = V_{cso} \tag{14}$$

Equations (15)-(17) are intermediate equations used in the state and output equations. Velocity components V_{csu}, V_{cwu}, V_{cfu}, V_{cso} and V_{cfo} are presented in Le Roux et al. (2013).

$$\varphi = \left(1 - \left(\frac{1}{\varepsilon_{sv}} - 1\right)\frac{X_{ms}}{X_{mw}}\right)^{0.5} \tag{15}$$

$$Z_x = \frac{X_{mw} + X_{mr} + X_{ms} + X_{mb}}{v_{mill} v_{P_{max}}} - 1 \tag{16}$$

$$Z_r = \frac{\varphi}{\varphi_{P_{max}}} - 1 \tag{17}$$

Table 2. Description of subscripts

Subscript	Description
$X_{\Delta -}$	f-feeder; m-mill; s-sump; c-cyclone
$X_{- \Delta}$	w-water; s-solids; c-coarse; f-fines; r-rocks; b-balls
$V_{- - \Delta}$	i-inflow; o-outflow; u-underflow

The mill power consumption is of interest in this study. The power that the mill motor supplies is given by (9). The relationship between mill load and power is often assumed to be parabolic (Craig et al. (1992), Powell et al. (2009), (2011)). In the case study presented here, an increase in load results in an increase in power up to when the mill is approximately 45 % full; when the load increases above this value, the power starts to decrease.

3. CONTROL FORMULATION

3.1 Control Objectives

As discussed earlier, the main control objectives for this new formulation is to achieve both a good *'quality'* (product size or PSE) and good *'quantity'* or throughput (THP). An additional advantage of minimizing power was also studied.

The control configuration is shown in Fig 2 where the difference between the NMPC Base and NMPC Opt is the energy term in the cost function. Effectively, the goal for the optimized case is to minimize the largest contributors to power consumption, i.e. α_{speed}, while still maintaining the desired set-points for PSE, LOAD and THP.

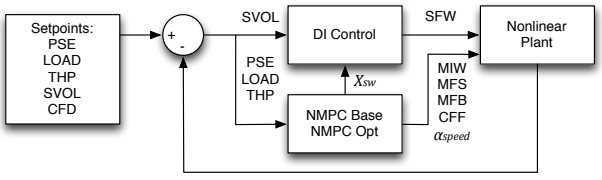

Fig. 2. Block diagram illustrating control configuration implemented.

3.2 Nonlinear model predictive control (NMPC)

The MPC controller was designed using the full nonlinear state space equations as described in Section 2.3. The objective of the controller is given by (18) where $\mathbf{u}$ represents the manipulated variables to solve the nonlinear optimal control problem by minimizing a performance index (J).

In (18)-(27), $\mathbf{x}$ are the states with initial values $\mathbf{x}_0$, $\mathbf{y}$ refers to the controlled variables, $\mathbf{y}_{sp}$ refers to the set-points, and $\mathbf{p}$ refers to the parameter values for the system.

$$\min_{\mathbf{u}} J(\mathbf{u}, \mathbf{x}_0, \mathbf{p}) \tag{18}$$

$$\text{s.t. } \mathbf{y} \in \mathbb{Y}, \mathbf{u} \in \mathbb{U} \tag{19}$$

$$\dot{\mathbf{x}}(t) = f(\mathbf{x}(t), \mathbf{x}(t - (\tau_{sc} + \tau_{cm})), \mathbf{u}(t), \mathbf{u}(t - (\tau_{sc} + \tau_{cm})), \mathbf{p}) \tag{20}$$

$$\mathbf{y}(t) = g(\mathbf{x}(t), \mathbf{x}(t - \tau_{sc}), \mathbf{u}(t), \mathbf{u}(t - \tau_{sc}), \mathbf{p}) \tag{21}$$

$$\tau_{sc} = 30s, \tau_{cm} = 10s \tag{22}$$

$$\mathbf{u} = \{MIW, MFS, MFB, CFF, \alpha_{speed}, X_{sw}\}^T \tag{23}$$

$$\mathbf{y} = \{PSE, LOAD, THP\}^T \tag{24}$$

$$\mathbb{Y} = \{\mathbf{y} \in \mathbb{R}^{n_y} | \mathbf{y}_l \leq \mathbf{y} \leq \mathbf{y}_u\} \tag{25}$$

$$\mathbb{U} = \{\mathbf{u} \in \mathbb{R}^{n_u} | \mathbf{u}_l \leq \mathbf{u} \leq \mathbf{u}_u\} \tag{26}$$

$$\begin{aligned} J(\mathbf{u}, \mathbf{x}_0, \mathbf{p}) = &\sum_{n=1}^{N_p} (\mathbf{y} - \mathbf{y}_{sp})^T \mathbf{Q}_1 (\mathbf{y} - \mathbf{y}_{sp}) \\ &+ \sum_{n=1}^{N_p} \Delta \mathbf{y}^T \mathbf{Q}_2 \Delta \mathbf{y} \\ &+ \sum_{n=1}^{N_c} \Delta \mathbf{u}^T \mathbf{Q}_3 \Delta \mathbf{u} + q_4 \sum_{n=1}^{N_p} \frac{P_{mill}}{P_{max}} \end{aligned} \tag{27}$$

The upper and lower constraints for the CVs are given by $\mathbf{y}_u$ and $\mathbf{y}_l$ respectively and are shown in Table 1. Similarly, for the input vector, $\mathbf{u}_u$ and $\mathbf{u}_l$ are also included.

The prediction horizon (N_p) should be chosen based on the longest settling time between the manipulated and controlled variables (Seborg et al. (2004)). This would result in a $N_p > 500$ due to the PSE-α_{speed} combination. For practical purposes a N_p value of 18 was chosen which corresponds to a 3 minutes prediction. One control move was implemented and kept constant for the prediction horizon, this showed good results. α_{speed} has been included as a control variable to control PSE and THP effectively. THP is regarded as an important control variable and given a larger weight. α_{speed} has been constrained between 0.7 and 1. Rate constraints on outputs have been included. Note that for the base case simulation the weight for power was set to zero. The matrices $\mathbf{Q}_1$, $\mathbf{Q}_2$, $\mathbf{Q}_3$ and q_4 represent the weights for the CVs, rate of the CVs, rate of MVs and power term respectively. These are significant differences from to the robust NMPC presented in Coetzee et al. (2010). The output weights were chosen based on the goal to achieve a high throughput and high quality. The input weights were chosen based on the maximum acceptable movement of an input variable.

$$\mathbf{Q}_1 = diag(q_1, q_2, q_3) \tag{28}$$

$$q_1 = \frac{\bar{q}_1}{y_{1_{max}}^2}, y_{1_{max}} = 2.5, \bar{q}_1 = 200 \tag{29}$$

$$q_2 = \frac{\bar{q}_2}{y_{2_{max}}^2}, y_{2_{max}} = 6, \bar{q}_2 = 20 \tag{30}$$

$$q_3 = \frac{\bar{q}_3}{y_{3_{max}}^2}, y_{3_{max}} = 5, \bar{q}_3 = 200 \tag{31}$$

$$\mathbf{Q}_2 = 10^{-3} diag\,(q1, q2, q3) \tag{32}$$

$$\mathbf{Q}_3 = diag(r_1, r_2, r_3, r_4, r_5, r_6) \quad (33)$$

$$r_1 = \frac{\bar{r}_1}{r_{1_{max}}^2}, r_{1_{max}} = 50, \bar{r}_1 = 10^{-5} \quad (34)$$

$$r_2 = \frac{\bar{r}_2}{r_{2_{max}}^2}, r_{2_{max}} = 100, \bar{r}_2 = 10^{-5} \quad (35)$$

$$r_3 = \frac{\bar{r}_3}{r_{3_{max}}^2}, r_{3_{max}} = 2, \bar{r}_3 = 10^{-4} \quad (36)$$

$$r_4 = \frac{\bar{r}_4}{r_{4_{max}}^2}, r_{4_{max}} = 50, \bar{r}_4 = 10^{-5} \quad (37)$$

$$r_5 = \frac{\bar{r}_5}{r_{5_{max}}^2}, r_{5_{max}} = 0.2, \bar{r}_5 = 10^{-5} \quad (38)$$

$$r_6 = \frac{\bar{r}_6}{r_{6_{max}}^2}, r_{6_{max}} = 2, \bar{r}_5 = 10^{-4} \quad (39)$$

The weight q_4 was only implemented in the optimized simulation and not in the base case simulation.

$$q_4 = 18 \quad (40)$$

3.3 Dynamic Inversion (DI)

The sump volume has traditionally been controlled using single loop PID. From (6), it is clear that there are nonlinear dynamics. Dynamic inversion was chosen because of its simple design and easy online implementation. This method leads to a closed form solution for the controller and guarantees asymptotic stability for the error dynamics (Enns et al., 1994). Dynamic inversion was used for SVOL and X_{sw} control. The desired X_{sw} value is fed from the MPC. In this way, the two controllers could be said to be coupled with one another. SFW has the largest impact on both these values and was therefore used as the manipulated variable. Dynamic inversion allows the specification of a desired response path by choosing a proportional gain value (K_p) and an integral gain value (K_I) such that: $\dot{E} + K_p E + K_I \int_0^t E d\tau = 0$ where $E = Y - Y^*$ (the difference between the measured value ($\dot{Y}$) and the setpoint (Y^*)). For SVOL control, (41) results where $E = \Delta S_{vol} = SVOL - SVOL^*$. Equation (42) results from algebraic manipulation and solving for the control variable SFW.

$$\frac{d}{dt}(\Delta S_{vol}) + K_p(\Delta S_{vol}) + K_I \int_0^t (\Delta S_{vol}) d\tau = 0 \quad (41)$$

$$SFW_{SVOL} = (CFF - V_{swi} - V_{ssi}) - K_p(\Delta S_{vol}) - K_I \int_0^t (\Delta S_{vol}) d\tau \quad (42)$$

K_p was chosen to be 30, this was based on a desired settling time of approximately 2 minutes. K_I was chosen to be ten times less than K_p. This resulted in good sump volume control without exceeding any input constraints on SFW. The sump level was to be maintained between 2 and 9.5 m^3. The K_p value is significantly larger than expected due to the sampling time of 10 seconds.

Similarly for sump water (X_{sw}) control: $E = \Delta X_{sw} = X_{sw} - X_{sw}^*$. The solution for SFW is shown in (43).

$$SFW_{X_{sw}} = \frac{CFF X_{sw}}{X_{sw} + X_{ss}} - \frac{V_V \phi X_{mw}^2}{X_{ms} + X_{mw}} - K_I \int_0^t (\Delta X_{sw}) d\tau - K_p(\Delta X_{sw}) \quad (43)$$

K_p was chosen to be ten times as much as the SVOL K_p value. The K_I value was also chosen to be ten times less than the K_p.

A convex combination of SFW_{SVOL} and $SFW_{X_{sw}}$ was chosen for smooth control of both outputs. This convex combination is shown in (44).

$$SFW = (1 - \lambda) SFW_{X_{sw}} + \lambda SFW_{SVOL} \quad (44)$$

$$\lambda(SVOL) = \begin{cases} 0 & \text{if } LB < SVOL < UB \\ \frac{1}{Min - LB}(SVOL - LB) & \text{if } Min \leq SVOL \leq LB \\ \frac{1}{Max - UB}(SVOL - UB) & \text{if } UB \leq SVOL \leq Max \\ 1 & \text{if } SVOL < Min \text{ or } SVOL > Max \end{cases}$$

$$\text{Lower Bound}(LB) = 3.25, \text{Upper Bound}(UB) = 8.25, Minimum = 2, Maximum = 9.5 \quad (45)$$

4. RESULTS

4.1 Simulation setup

To illustrate the control capability and the effect of including an energy factor in the nonlinear MPC objective function, an 8 h and 24 h simulation run was performed using the control formulation described in Section 3. Dynamic inversion and a nonlinear MPC was used to control a nonlinear ROM ore milling circuit described in Section 2.3. A sampling time of 10 seconds was used for the simulation. State estimation is not the focus of this paper and full state feedback is assumed. In practice, observers will have to be used as all states are not measured, see e.g. (Olivier et al. (2012)). Also, this study aims to show the control accuracy and not the noise-handling capability. An additional constraint on α_{speed} was added to ensure smooth control: $\Delta\alpha_{speed} \leq 0.005$.

The implementation of time delays was achieved by utilizing previous state values in the state vector. The *fmincon* function requires an objective function and can cater for various constraint functions (such as equality and inequality constraints). Within the objective function, the states and outputs of the mill and sump are propagated (which are a function of the control moves). The outputs are checked if they are within equality constraints defined in the constraints function. The constraints function comprises of inequality input and output constraints defined in Table 1.

4.2 Control accuracy

Two disturbances and one set-point change was applied during the 8 h simulation. Additional spillage water was added to the sump between 2 h and 2.5 h with a magnitude of 30 m^3/h. The MIW was reduced by 10 m^3/h from 4 h to 4.5 h to simulate an input pipe leak. A THP set-point change was made at 6 h moving from 88 t/h to 90 t/h, PSE and LOAD remained constant.

Figure 3 illustrates how well the control configuration performs with disturbances and a set-point change. The sump volume is within the desired limits.

Figure 4 illustrates how well the nonlinear dynamic inversion control technique operates.

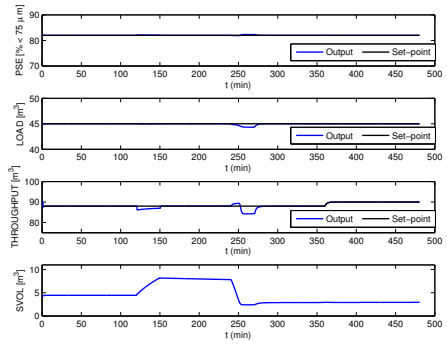

Fig. 3. Output variables and set-point tracking

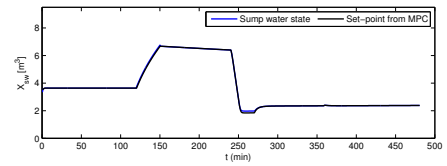

Fig. 4. Dynamic inversion control. Desired and output value for the hold-up of sump water.

It should be noted that all the manipulated variables and other important variables such as the power output, rheology factor and the cyclone feed density are within acceptable regions.

4.3 Power consumption comparison

Various set-point changes were made to the throughput (THP) and particle size (PSE) every 4 hours. The total charge of the mill (LOAD) was kept constant at 45% full. An energy factor was added to the nonlinear MPC to illustrate the additional possibilities that this control configuration possesses. The results show that the power from the mill is tightly linked with the circuit outputs i.e. changing P_{mill} will have a direct effect on whether the outputs reach set-point. The power consumed by the pump, after the sump, was regarded as negligible compared to the power consumed by the mill.

In the first run, the energy factor was not taken into account ($q_4 = 0$). The weight q_4 was introduced in the second simulation run with a starting value of 30. The error between the PSE measured value and the set-point value was determined every hour and if the error was larger than 0.1 %, the run was flagged as unsuccessful. Similarly for THP, an unsuccessful run resulted if the THP error was larger than 1 %. Once a run was flagged as unsuccessful, the run was restarted with a new q_4 value. The new q_4 value is 90 % smaller than the previous q_4 value.

The results show that in 24 h, and an energy term weight (q_4) of 18, a 332.7 kWh reduction in energy resulted with a 0.6% drop in THP and 0.1% drop in PSE. These results shows that the system is tightly integrated with power and that if the end result is to minimize power, there will, as expected, have to be some sacrifice in THP or PSE. The energy difference was calculated using the trapezoidal rule for the P_{mill} output variable.

Figure 5 shows the difference in P_{mill} between the base case ($q_4 = 0$) and the minimized energy case ($q_4 = 18$). Figure 6 illustrates the difference in the additional outputs, rheology factor and cyclone feed density. The rheology factor shows very similar outputs while the density shows a slight change.

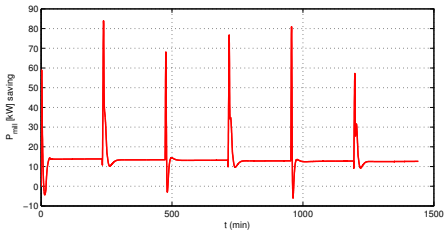

Fig. 5. P_{mill} output difference between base case and optimized case in kW. Optimized case contains energy factor in NMPC objective function.

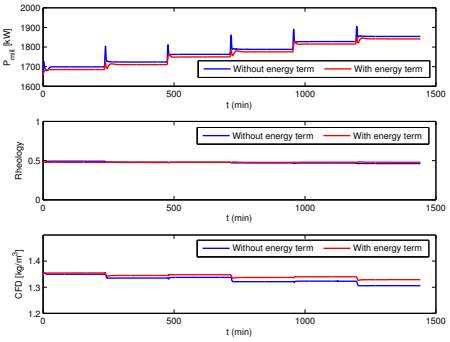

Fig. 6. Output variables for base case and optimized case simulation.

PSE, THP and LOAD tracking is shown in Fig. 7. In the second run, the LOAD is around 47% full. This result conforms with the model, the P_{mill} value is reduced as the mill load moves away from 45% full.

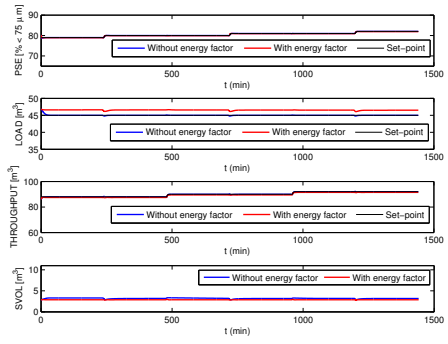

Fig. 7. Controlled variables for base case and optimized case simulation.

Figure 8 shows the dynamic inversion controller tracking the X_{sw} set-point from the MPC. The energy factor run shows the effect of the convex combination (described in (44)). A compromise in reaching the desired X_{sw} can be seen due to the prevention of the sump running dry.

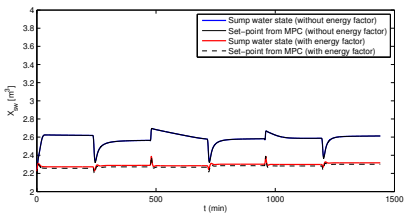

Fig. 8. Dynamic inversion control for base case and optimized case.

Figure 9 and 10 show that the manipulated variables are all within constraints.

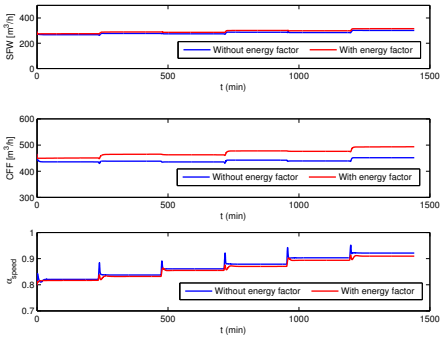

Fig. 9. Manipulated variables for base case and optimized case simulation.

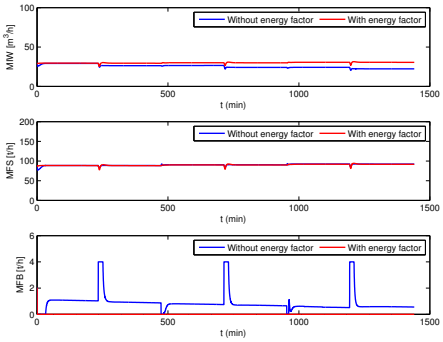

Fig. 10. Manipulated variables for base case and optimized case simulation.

Depending on the product processed and the type of mill used, the cost of electricity may be significantly less than the value of the product produced. However, as the cost of electricity increases the re-evaluation of cost-vs-profit will be worthwhile. The results show that this milling circuit model is close to power optimized when including α_{speed} as a manipulated variable.

5. CONCLUSION

A combined nonlinear dynamic inversion and nonlinear model predictive control design approach is followed in this paper to propose a new effective control design philosophy for complex milling circuits, which meets the ambitious objectives of high product quality, high throughput, manageable loads in the mill as well as minimizing the power consumption for the mill. Effectiveness of the proposed approach has been demonstrated by taking various combinations of throughput, PSE and load. A study has also been carried out to demonstrate the power savings by lowering product quality and/or throughput, which is not reported due to space constraints. It can be noted that recent studies show that power can be saved by implementing a real time optimizer on a supervisory outer-loop level. This paper, on the other hand, tries to save energy in the inner loop (by additionally penalizing an energy factor as part of the cost function). Hence, there is a scope to combine the two philosophies to obtain a better energy savings, which is a topic for future research. Future research should also contain noise and effects of modeling errors.

REFERENCES

Bauer, M. and Craig, I.K. (2008). Economic assessment of advanced process control - A survey and framework. *J. Process Control*, 18(1), 2–18.

Chen, X., Zhai, J., Li, S., and Li, Q. (2007). Application of model predictive control in ball mill grinding circuit. *Minerals Eng.*, 20(11), 1099 – 1108.

Coetzee, L., Craig, I., and Kerrigan, E. (2010). Robust nonlinear model predictive control of a run-of-mine ore milling circuit. *IEEE Transactions on Control Systems Technology*, 18(1), 222 –229.

Craig, I., Hulbert, D.G., Metzner, G., and Moult, S.P. (1992). Optimized multivariable control of an industrial run-of-mine circuit. *Journal of the South African Institute of Mining and Metallurgy*, 2, 169 176.

Craig, I. and MacLeod, I. (1996). Robust controller design and implementation for a run-of-mine ore milling circuit. *Control Engineering Practice*, 4(1), 1 – 12.

Enns, D., Bugajski, D., Hendrick, R., and Stein, G. (1994). Dynamic inversion: an evolving methodology for flight control design. *International Journal of Control*, 59(1), 71–91.

Le Roux, J., Craig, I., Hulbert, D., and Hinde, A. (2013). Analysis and validation of a run-of-mine ore grinding mill circuit model for process control. *Minerals Engineering*, 43-44, 121–134.

Matthews, B. and Craig, I. (2013). Demand side management of a run-of-mine ore milling circuit. *Control Engineering Practice*, 21(6), 759–768.

Olivier, L. and Craig, I. (2013). Model-plant mismatch detection and model update for a run-of-mine ore milling circuit under model predictive control. *Journal of Process Control*, 23(2), 100–107.

Olivier, L., Huang, B., and Craig, I. (2012). Dual particle filters for state and parameter estimation with application to a run-of-mine ore mill. *Journal of Process Control*, 22(4), 710 – 717.

Powell, M., Perkins, T., and Mainza, A. (2011). Grindcurves applied to a range of sag and ag mills. In *Proceedings of SAG 2011*. Vancouver, BC, Canada.

Powell, M., van der Westhuizen, A., and Mainza, A. (2009). Applying grindcurves to mill operation and optimisation. *Minerals Eng.*, 22(78), 625632.

Seborg, D.E., Edgar, T.F., and Mellichamp, D.A. (2004). *Process dynamics and control*. NJ: Wiley, 2nd edition.

Wei, D. and Craig, I.K. (2009). Grinding mill circuits - a survey of control and economic concerns. *International Journal of Mineral Processing*, 90(14), 56 – 66.